Impurity-breakdown-induced current filamentation in a dipolar electric field

V. Novák,* C. Wimmer, and W. Prettl
Institut für Experimentelle und Angewandte Physik, Universität Regensburg, 93040 Regensburg, Germany
(Received 8 December 1994; revised manuscript received 6 April 1995)

Filamentary current flow has been investigated in an epitaxial *n*-type GaAs layer with two Ohmic point contacts. A scanning laser microscope technique has revealed two characteristic regimes of filamentary structure: a large-area filament typical at higher sample currents, and a bendable filament arising at low currents and becoming curved in perpendicular magnetic fields. Self-organization is supposed to be significant upon forming the bendable filament, whereas the large-area filamentary structure is predominantly formed by the electric field distribution due to the point contact geometry. Numerical simulations have been carried out in the second case, showing a good agreement with experimental results.

I. INTRODUCTION

Spontaneous formation of channels of high conductivity, namely current filaments, has been observed in a wide range of semiconductor materials and structures. There are several physical mechanisms that can be found in the background of this phenomenon. Besides the pinch effect and the electron overheating effect,[1] known from plasma physics and typical for very high current densities, another class of mechanisms leading to current filamentation has been proposed: an analogy to reaction-diffusion phenomena of chemical systems.[2–5] Accordingly the reaction kinetics between different electron energy states may be described by a system of rate equations which, coupled with Poisson's equation and the continuity equation, yields spatially inhomogeneous solutions. This description seems to be the most appropriate one in the case of filamentary structures, which can be observed in the regime of impurity breakdown at low temperature.

Various methods have been used to visualize the spatially inhomogeneous current flow. Among them, noninvasive techniques seem to be preferable, such as temperature or potential measurement[6] or scanning of recombination radiation.[7] However, both methods are inapplicable in the case of low-temperature impurity breakdown because of technical difficulties or insufficient intensity of radiation, respectively. So far the most convincing results under these conditions have been achieved by low-temperature scanning electron microscopy[8–10] and its laser beam analogy.[11,12] Both are based on some kind of interaction between the investigated structure and a testing device. The exact physical mechanism of this interaction is, however, not yet fully understood. It cannot be generally excluded that its influence is detrimental to the observed structure. Thus, the applicability of these strongly invasive imaging methods seems to be confined to stationary and sufficiently stable filamentary patterns.

Such states have been found and investigated in epitaxial layers of *n*-type GaAs with a fundamentally inhomogeneous electric field imposed by some specific contact geometry. In this paper, the investigation of a sample with a pair of point contacts is reported. After a brief explanation of the principles of the laser beam imaging method, the reconstructions of filamentary structures in the post-breakdown regime will be presented in the experimental section. The attention will be drawn to some characteristic properties, which enable us to distinguish between two different regimes of a current filament. In one of them, the role of an externally imposed electric field distribution will be shown to be substantial. In the theoretical section, a one-dimensional model of the cross section of a filamentary structure in this regime will be designed based on the two-level model by Schöll.[3,5] The basic stationary effect of a perpendicular magnetic field will be allowed for also.

II. EXPERIMENTAL RESULTS

A. Experimental setup

The experimental setup of the scanning laser microscope mentioned above is shown in Fig. 1. The spatially filtered beam of an interband light laser was scanned across the surface of the biased sample by a mechanical deflection unit. The beam was focused on the sample surface to a spot diameter of about 30 μm. The light power was adjustable up to 0.5 mW in the focus plane. Si-

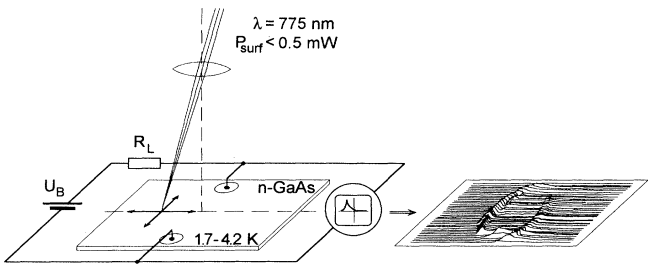

FIG. 1. Setup of scanning laser microscope (Ref. 12).

multaneously with the scanning, the sample current was recorded. It turns out that the interfaces between the regions of high and low conductivity are most sensitive to focused illumination. Several phenomena seem to be involved in the light induced reaction: besides a stationary increase in the sample current, a nonstationary, pulselike component of varying amplitude and repetition rate is usually present.[13] With an optimally adjusted light intensity, a signal of less then 10-mV amplitude can be obtained superimposed on the sample voltage. After time averaging or lock-in detection, the two-dimensional mapping of the light induced signal can be reconstructed, reflecting the position of the boundaries of the filamentary structure. A detailed investigation of the underlying physical mechanism is being carried out and will be reported elsewhere.

All experimental results reported here have been obtained on a sample of an n-type conducting epitaxial layer of GaAs grown by liquid-phase epitaxy on semi-insulating Cr-doped GaAs substrate. Two pairs of Ohmic point contacts were alloyed into the epitaxial layer. Parameters of the sample are summarized in Table I. They are not critical for the observed phenomena: Similar results have been obtained on other n-type GaAs samples.

The sample was mounted in an optical immersion cryostat and cooled to 1.8 K. A magnetic field could be applied perpendicular to the epitaxial layer by a superconducting magnet. A bias voltage was supplied to the sample in series with a load resistor.

Figure 2 shows the voltage-current characteristics of the sample. For low bias voltages, the sample is practically nonconductive as all electrons are captured in the impurity states. At a certain critical bias voltage, an avalanche breakdown of shallow impurities occurs, free electrons are multiplied, and the sample becomes conductive. The back transition from the conductive to the nonconductive phase is hysteretically shifted, which forms a broad region of bistability. The process of transition between the two states is influenced by the value of the load resistor. For the resistance greater than some critical value, the system becomes unstable and undamped relaxation oscillations arise in the breakdown regime.[14]

A perpendicular magnetic field modifies the I-V curve in two ways. First, the conductivity of the sample decreases at higher currents, which may well be attributed to the effect of magnetoresistivity. Second, the I-V curve is deformed in a complex way at lower currents and a new hysteretic curve arises in the immediate post-breakdown regime. As will be discussed in more detail later, this effect is to be attributed to the presence of the additional, inactive pair of contacts on the sample.

TABLE I. Geometry and material parameters of the sample.

Sample dimensions		4.1×3.7 mm
Contact distance	c	3.5 mm
Contact radius	R	< 0.5 mm
Layer thickness		29 μm
Donor density	N_D	11.9×10^{14} cm^{-3}
Compensation ratio	N_A/N_D	0.91
Free electron density at 77 K	n	9.6×10^{13} cm^{-3}
Electron mobility at 77 K	μ_n	4.5×10^4 cm^2 V^{-1} s^{-1}

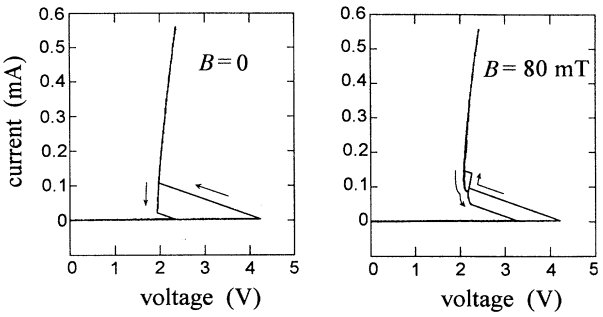

FIG. 2. Current-voltage characteristics of the sample without and with a magnetic field normal to the epitaxial layer.

B. Filament reconstructions: Regime of large-area filament

The filament images shown in Fig. 3 have been recorded in a regime well above the threshold of breakdown. The laser light power incident in the sample was about 0.2 mW, approximately one order of magnitude lower than the Joule heating in this regime. As mentioned above, the two ridgelike structures in each of the mappings correspond to the boundaries of a convex-shaped region with significantly higher conductivity. Not surprisingly, the width of this region rises with increasing current. This can be seen from Fig. 4, where only one middle line of the filament reconstruction is plotted for a range of sample currents.

An important conclusion can be readily made: the shape of this current filament indicates the significant role of the electric field distribution. Unlike the effect of current contracting mechanisms, known, e.g., from plasma physics, and unlike some previously observed fila-

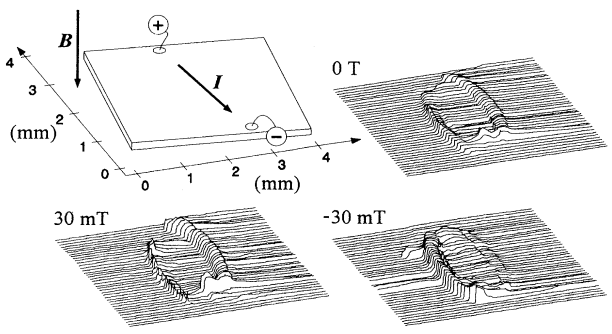

FIG. 3. The reconstructions of large-area filaments. The sample was biased in series with 1 kΩ load resistor. The stationary current was 1 mA.

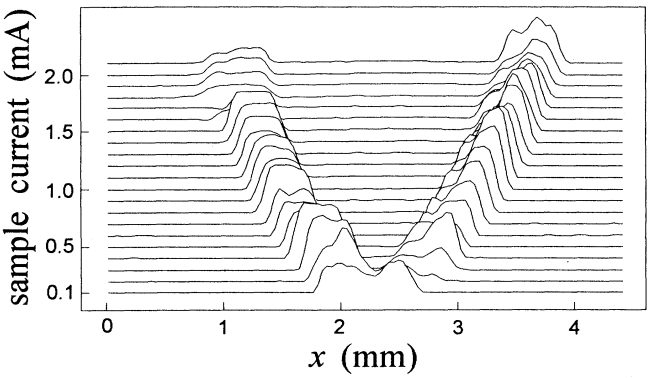

FIG. 4. The filament width for various sample currents. In the figure the central lines of filament reconstructions are plotted.

mentary structures,[9,10] the width of the investigated filament reaches an apparent maximum halfway between the contacts; the shape of the filament boundaries resembles the course of field lines in an undisturbed dipolar electric field from the sample contacts. Moreover, the same shape of a free filament wall can be found in samples where the other wall is fixed by a sample edge lying close to the contacts (Fig. 5). Thus, the formation of one filament boundary seems to be practically independent on the character and precise location of the second one.

The response of the filamentary structure to a perpendicular magnetic field yields additional support to the conclusion on the essential role of the distribution of electric field strength. While the symmetry in the *form* of the response of opposite filament boundaries is lost (see Fig. 3 bottom), the boundaries themselves exhibit no or negligible sideshift, as could have been expected due to the Lorentz force.

Consequently, the dipolar electric field must be assumed to efficiently stabilize the macroscopic shape of the current filament in the investigated case. Moreover, the field distribution appears to be insignificantly disturbed by the presence of a conductive area of the current filament. The opposite boundaries of this conductive region are formed independently from each other. Since this is obviously possible only if the separation between them is in a certain sense large enough, we call this type of filamentary structure large-area filament.

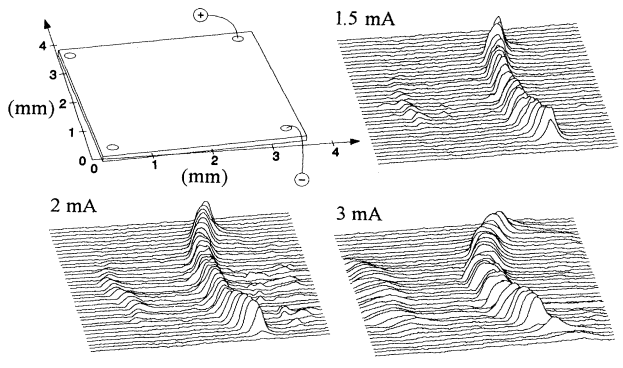

FIG. 5. The reconstructions of large-area filaments constrained by a sample edge for a range of sample currents. The less apparent structure at the left of the sample stems from the second pair of contacts, which was not completely isolated.

C. Filament reconstructions: Regime of bendable filament

The filament reconstructions shown in Fig. 6 have been obtained on the same sample as in Fig. 3, but with a bias just above the impurity breakdown voltage. Because of the essentially lower stability of the filamentary structure in this regime, the illumination had to be reduced by using only 25-ns short light pulses at the repetition rate of typically 20 Hz. This gave an average light power of 10^{-3} mW, which is again significantly smaller than the Joule heating for the present biasing condition. Since the nonstationary component of the induced signal increased significantly at the same time, a careful time averaging of the recorded signal had to be performed. In spite of it, the rather moderate quality of the reconstructions could not completely be eliminated.

Besides the expectedly reduced width of the filament, which leads to an overlap in the imaging response of both filament boundaries, another effect can be recognized: a bending of the current filament in the direction of the Lorentz force. This effect distinguishes most apparently the low-current filamentary regime from the regime of large-area filament described in the previous section. In Fig. 7 only one middle line of the filament reconstruction is plotted for various magnetic field strengths. Whereas the large-area filament in Fig. 7(a) exhibits a negligible side shift even for higher magnetic fields, the displacement in the middle of the narrow filament is apparent and approximately proportional to the magnetic field strength in a range of ± 40 mT, Fig. 7(b).

Attention is to be given to the characteristic deformation of voltage-current characteristic in the presence of a perpendicular magnetic field, as shown in Fig. 2. Besides the effect of magnetoresistivity, a new hysteretic loop ap-

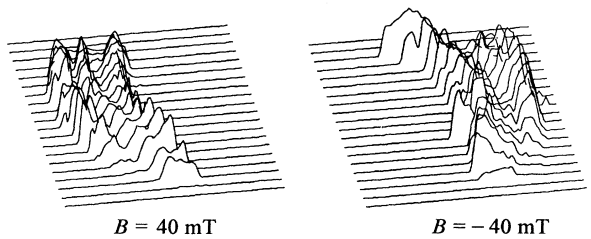

FIG. 6. The reconstructions of filament in perpendicular magnetic field in immediate post-breakdown regime. The sample was biased via a load resistor of 100 kΩ. The stationary current was 100 μA.

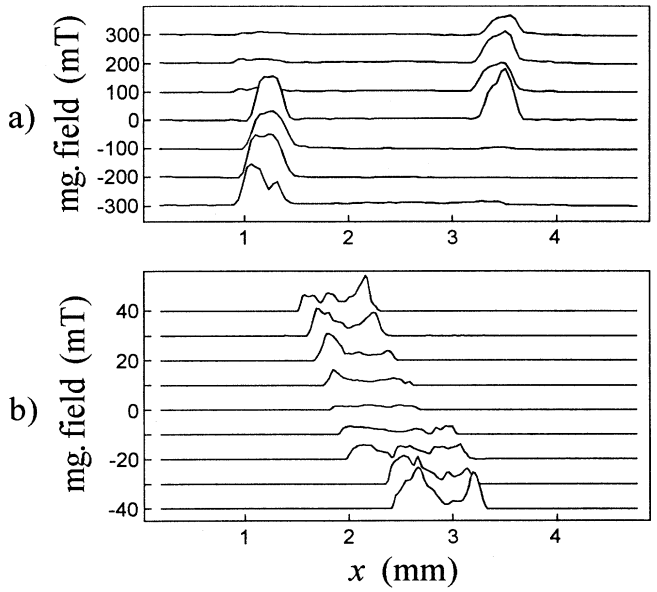

FIG. 7. Response of large-area filament (a) and bendable filament (b) to perpendicular magnetic field. Only the middle lines of the respective reconstructions are plotted. The sample was biased via 100-kΩ load resistor. The stationary currents were (a) 1.5 mA and (b) 0.1 mA, respectively.

pears in the immediate post-breakdown regime. Since the same phenomenon has been observed on various samples with the point contact geometry, a hypothesis has been recently proposed that the two stable states of the hysteretic region correspond to the large-area filament and to the low-current bendable filament, respectively.[13] This idea has to be revised. The occurrence of this bistability turns out to be uniquely correlated to the usual geometrical arrangement of the contacts in the corners of the sample (as in Fig. 5) or amid the sample edges (as, in fact, is the case in Fig. 3). No such bistability could have been found neither on samples without any additional contacts in the possible vicinity of the filament, nor in small magnetic fields. Thus, the effect is most probably explained through the presence of an electrically inactive contact near the middle of the maximally bent filament. At some critical bending, the filament gets obviously pinned to the relatively large, highly conductive region of the floating contact, and separates later discontinuously with rising current.

III. MATHEMATICAL MODEL

The thickness of an epitaxial layer in the order of 10 μm enables us to consider the current flow in two dimensions only. Further we will show that the typical properties of the large-area filament make it possible to reduce the essential part of the mathematical description to a one-dimensional problem. It should be stressed, however, that the simplifications accepted in the following text are questionable in the case of bendable filament. In that case, as well as in all nonstationary filamentary states, the full two-dimensional treatment is inevitable, which will not be treated here.

Let us adopt the coordinate system according to Fig. 8, with the y axis in the direction linking the two contacts and the x axis crossing the filament halfway between the contacts. As discussed above, the following two assumptions are experimentally justified in the large-area filament: (i) the filament walls of a large-area filament follow approximately lines of a constant electric field, leaving thus the dipolar field distribution between the two point contacts essentially unperturbed; (ii) the large-area filament is approximately symmetric with respect to reflection in the axis perpendicular to the contact dipole, i.e., with respect to the x coordinate.

The symmetry about the x coordinate implies that on this axis all derivatives (except the potential) in the y direction tend to zero. Consequently, the y components of the current density and the field strength vector vanish and an autonomous one-dimensional subsystem can be extracted from the physically two-dimensional problem: the cross section along an axis transversal to the current flow. This fact enables us to adopt basically the same one-dimensional mathematical apparatus, which was used by Schöll[3–5] to investigate the filamentary structures in a *homogeneous* E_y field.

The governing equations for an n-type semiconductor in a steady state are Poisson's equation for the electric potential ψ

$$\frac{d^2\psi}{dx^2} = -\frac{\rho}{\varepsilon_S} = -\frac{e}{\varepsilon_S}\left(N_D^+ - N_A^- - n\right) \tag{1}$$

and the transport equation for the current density J_{nx} in the x direction

$$J_{nx} = -e\,\mu_n n\frac{d\psi}{dx} + e\,D_n\frac{dn}{dx}, \tag{2}$$

where ρ is charge density, ε_S is the permitivity of the semiconductor, N_D^+ and N_A^- are the densities of ionized donor and acceptor impurities, respectively, n is the free electron concentration, μ_n is the electron mobility, and D_n is the diffusion constant.

The continuity equation in a steady state degenerates into the requirement of spatially constant current density J_{nx}. Physical reasonableness leads then to the condition $J_{nx}(x) = 0$ along the x axis. Upon integrating the transport equation, the simple relation between the

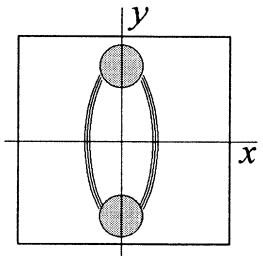

FIG. 8. Coordinate system of the model.

free electron density n and the electric potential ψ can be derived

$$n(x) = n_0 \exp \frac{\psi(x)}{u_T}, \tag{3}$$

provided that the Einstein relation $D_n = u_T \mu_n$ holds; u_T is the thermal potential, $u_T = k_B T/e$, and n_0 is the free electron density in a reference point x_0, $\psi(x_0) = 0$.

It has been shown that the presence of two levels of localized states in addition to the conduction band is necessary and sufficient to yield a system with up to three equilibrium states, which differ in free electron density.[5] Consequently, the material shows an S-shaped relation between current density and electric field strength (J–E characteristic), which is known to be typical for the occurrence of spatially inhomogeneous steady states in the form of current filaments.[1,15] In the case of n-type GaAs at liquid helium temperature, the ground state and the first excited state of shallow donors are involved in the most probable transition processes, which are shown in Fig. 9. The transition rates can be described in analogy with chemical reaction kinetics in the following form:[5]

$$\begin{aligned} \dot{n}_D^* &= T_1^S N_D^+ n + X^* n_D - X_1^S n_D^* - X_1^* n_D^* n - T^* n_D^*, \\ \dot{n}_D &= T^* n_D^* - X^* n_D - X_1 n_D n, \end{aligned} \tag{4}$$

where n_D and n_D^* are the electron densities in the ground and excited states, respectively. The impact ionization rate coefficients X_1 and X_1^* depend strongly on the electric field. For the sake of simplicity, these dependences are approximated by the semiempirical formula[16,17]

$$X_1 = X_\infty \exp\left[-\left(\frac{E_{\mathrm{av}}}{|\boldsymbol{E}|}\right)^\alpha\right], \tag{5}$$

where X_∞, E_{av}, and α are constants, and $|\boldsymbol{E}|$ is the local electric field strength. An analogous relation holds for X_1^*.

In a steady state, the rate equations (4) become algebraic and both n_D and n_D^* can be expressed as rational functions of n. Since $N_D^+ = N_D - n_D - n_D^*$ and all the acceptorlike impurities are assumed to be ionized, Eq. (1) can be rewritten into the form

$$\frac{d^2\psi}{dx^2} = \frac{P_3[\exp(\psi/u_T);\, E_y(x)]}{P_2[\exp(\psi/u_T);\, E_y(x)]}, \tag{6}$$

where P_2 and P_3 for simplicity denote second- and third-order polynomials, respectively. This nonlinear nonautonomous differential equation describes the distribution of an electric potential in the cross section of the current filament.

It is noted that through the relation (5) some of the coefficients in the polynomials P_2 and P_3 are functions of the magnitude of the local electric field strength $|\boldsymbol{E}| = \left[(d\psi/dx)^2 + E_y(x)^2\right]^{1/2}$. While the first derivative of the potential makes Eq. (6) nonlinear, the function $E_y(x)$, which reflects the field distribution, makes it nonautonomous. With respect to assumption (i) from the beginning of this section, $E_y(x)$ in a steady state is presumed to be given only by the geometry of the contacts and by the applied voltage. Two basic configurations can thus be distinguished: parallel stripelike contacts enforcing a spatially constant electric field, and the point or circular contacts with a dipolar field distribution. In the latter case, the y component of the electric field along the x axis is described by the decreasing function[18] (as long as the finite boundary effect may be neglected)

$$E_y(x) = \frac{U/\delta}{1 + (x/\sigma)^2}, \tag{7}$$

where U is the applied voltage, δ and σ are constants reflecting the contact diameter R and distance c between the contact centers in the following way:

$$\delta = \sigma \ln \frac{\sigma + (c/2 - R)}{\sigma - (c/2 - R)},$$

$$\sigma = \sqrt{(c/2)^2 - R^2}.$$

To avoid the uncertainty in the description of the physical boundary of the sample and to maintain the validity of Eq. (7), we choose the boundary points of the model to lie within the boundaries of the sample, but, at the same time, sufficiently far from them. Further, we constrain ourselves to such physically reasonable solution modes of Eq. (6), which tend to some homogeneous state far away from the filament boundaries. Such a homogeneous and thus charge neutral state corresponds to the trivial solution of Eq. (6)

$$P_3(n;\, E_y) = 0. \tag{8}$$

With the rate coefficients according to Table II, the cubic

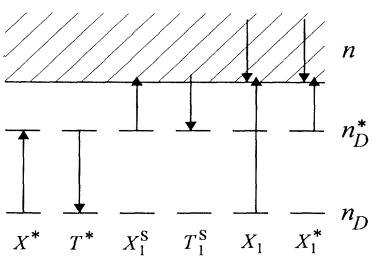

FIG. 9. The transition processes of two-level model (Ref. 5).

TABLE II. Numerical parameters of Eq. (6). The values of the rate coefficients are taken from Ref. 19 and correspond to a typical epitaxial layer of n-type GaAs at liquid helium temperature.

N_D	5.7×10^{20} m^{-3}	N_A	4.3×10^{20} m^{-3}
X^*	2.34×10^{6} s^{-1}	T^*	4.1×10^{7} s^{-1}
X_1^S	1.16×10^{6} s^{-1}	T_1^S	5.0×10^{-12} m^3 s^{-1}
$X_{1\infty}$	4.4×10^{-11} m^3 s^{-1}	$X_{1\infty}^*$	2.2×10^{-11} m^3 s^{-1}
E_{av}	244 V m^{-1}	E_{av}^*	122 V m^{-1}
α	2	α^*	2
σ	2.8 mm	δ	4.1 mm

equation (8) reveals an interval of bistability between E_h and E_{th} as shown in Fig. 10.

It can be seen that the values from the middle branch of the neutrality curve belong to the unstable homogeneous steady state, as its differential conductivity is negative. The remaining branches with $|\boldsymbol{E}| < E_{th}$ and $|\boldsymbol{E}| > E_h$ yield the values of electron density of a stable homogeneous state in a given electric field. Since the states on these branches are stable we can suppose that sufficiently slow spatial variations of local electric field E_y result only in slight deviations from the neutrality curve, as long as $|\boldsymbol{E}|$ does not exceed critical values E_{th} or E_h. Equations (7) and (8) can thus be used to define Dirichlet boundary conditions for Eq. (6), assuming the boundary points lie sufficiently far from the filament walls.

Basic solutions of Eq. (6) for several values of the bias voltage are shown in Fig. 11. It can be seen that there exists a certain critical value of a *local* field strength: when the component E_y decreases under this critical value, the density of free electrons suddenly falls, forming thus an edge of the highly conductive region. This conclusion corresponds to the basic result of Ref. 5 about coexistence of the low and high electron density regions in a homogeneous field with a *globally* constant critical electric field, namely, the coexistence field. For the given set of parameters, this coexistence field has been numerically found to agree exactly with the critical field as seen from Fig. 11.

The position of the filament boundary in the modeled case coincides with the point (i.e., the line in the plane) of the coexistence field; it shifts with changing bias. Assuming, in accordance with the presented model, some constant value E_{co} of this coexistence field, a simple square-root dependence of the filament width w on the applied voltage U can be derived through the inversion of Eq. (7)

$$w = 2\sigma\sqrt{\frac{U}{E_{co}\delta} - 1}. \tag{9}$$

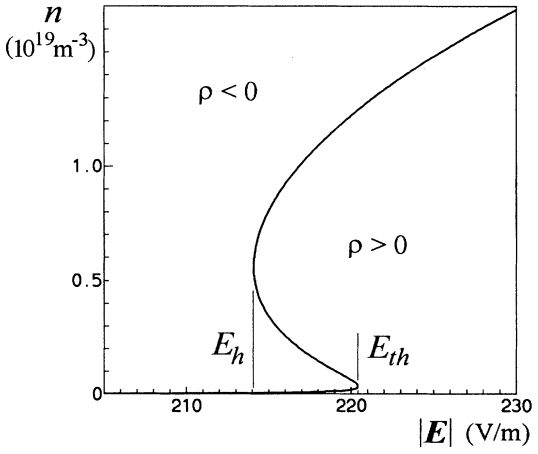

FIG. 10. Free electron density as a function of local electric field strength in a charge neutral state.

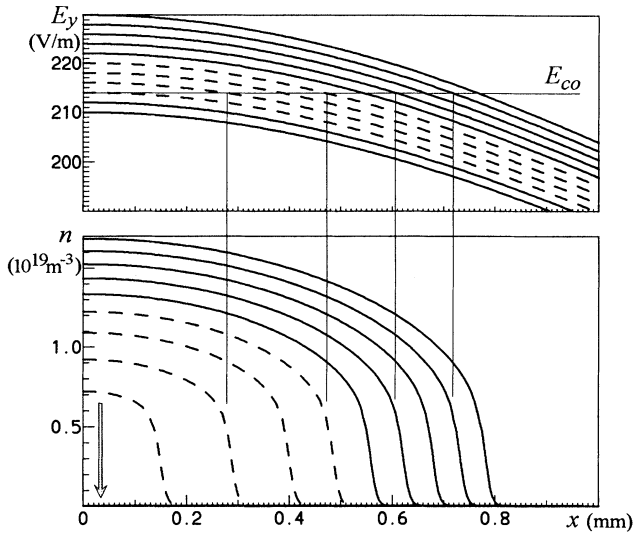

FIG. 11. The decay of the E_y component of the dipolar field in the transversal direction at several values of bias voltage (top) and the corresponding free electron profiles given by the solution of Eq. (6) (bottom); $x = 0$ lies in the longitudinal symmetry axis of the filament. At this point the E_y component of the electric field reaches its maximum proportional to the applied voltage according to Eq. (7). The dashed lines depict the bistable states in which the maximum of E_y does not exceed the interval of bistability and two values of n are possible as boundary values. The corresponding second stationary state with a low electron density lies always on the x axis within the resolution of the figure.

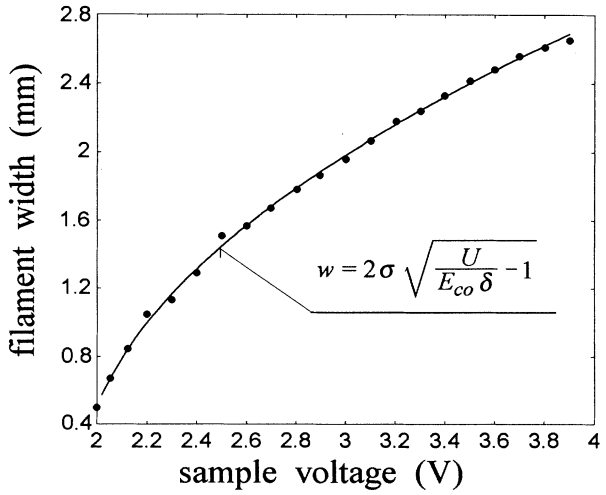

FIG. 12. Filament width as a function of applied voltage. The full circles indicate experimental data corresponding to Fig. 2. Parameters of the fitting curve (solid line) are $\sigma = 1.33$ mm and $E_{co}\delta = 1.93$ V, which correspond to an effective radius $R = 0.44$ mm and a distance between contacts $c = 2.8$ mm, cf. Table I.

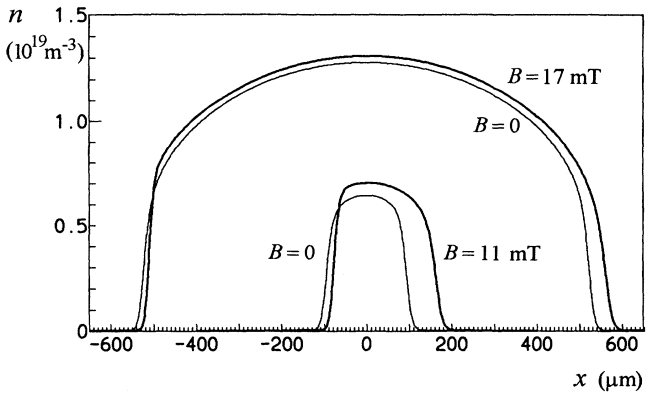

FIG. 13. Solutions of Eq. (6) in the presence of a magnetic field normal to the epitaxial layer. The thin lines show the solutions at the same bias but without magnetic field.

Using σ and δ as free parameters, (9) has been fitted to the experimental data of Fig. 4. A good agreement with the real dimensions of the sample, Fig. 12, justifies indirectly both of the assumptions (i) and (ii) from the beginning of this section.

It may finally be concluded that the shape of the filament as well as its position in a steady state are uniquely defined and stabilized by the field distribution. The role of self-organization is thus suppressed and confined only, on another spatial scale, to the formation of the phase interface, namely, the filament boundary.

To allow for the effect of a perpendicular magnetic field, an additional transport of free electrons in the x direction due to the Lorentz force can be phenomenologically described by introducing a new term into the transport equation (2)

$$J_{nx} = e\,\mu_n n E_x + e\,D_n \frac{dn}{dx} + \mu_H J_{ny}(x) B, \qquad (10)$$

where J_{nx} and J_{ny} are components of the current density vector, μ_H is the Hall mobility, and B is the magnetic induction. In a stationary state, if it exists, the J_{nx} component vanishes again, and the integration of (10) yields an analogy to (3)

$$\psi(x) = u_T \ln\left(\frac{n(x)}{n_0}\right) - \int_{x_0}^{x} E_H(x')\,dx', \qquad (11)$$

with the Hall field $E_H(x) = -\mu_H E_y(x) B$ and x_0 the reference point, $\psi(x_0) = 0$.

The solutions of Eq. (6) with the modification due to Eq. (10) are shown in Fig. 13. The loss of symmetry is apparent, especially in the case of the narrow filament. It should be stressed, however, that the results do not carry any information about the side displacement or bending of the filamentary structure; it is hidden in the not specified assumption of the vanishing lateral transport of electrons. Nevertheless, an analogy may be drawn from the case of a filament subject to a perpendicular magnetic field in a stripe contact geometry. In such a case, as found experimentally for p-type Ge,[20] the filament tends to travel laterally in the direction of the Lorentz force. Various mechanisms associated with this motion have been proposed, based, e.g., on different electron mobilities in the high- and low-conducting regions, respectively,[20] or on the disbalanced ionization and capture of free electrons on the opposite filament walls.[21,22] Irrespective of their actual nature, the same mechanisms must be supposed to act in our case, too, leading to the bending of the narrow filament and being balanced with a pinning effect of the point contacts.

IV. CONCLUSIONS

At low currents in the immediate post-breakdown regime, a narrow filamentary structure between two point contacts has been observed. The width of the structure lies in the order of resolution of the scanning laser microscope method. Subject to a perpendicular magnetic field, it exhibits an apparent bending in the direction of the Lorentz force, in an analogy with previously reported traveling of the filaments in a stripe contact geometry. Its maximum side displacement is approximately proportional to the applied magnetic field in the range of ± 40 mT.

With rising voltage bias, the filament width in a magnetic field free case increases in a square-root-like dependence. Simultaneously, the stability of the structure against an external perturbation grows and the influence of the perpendicular magnetic field on the lateral displacement decreases. Thus, at higher currents well above the breakdown another characteristic regime can be distinguished, in which the macroscopic shape of the filament is essentially determined by the inhomogeneous distribution of the electric field imposed by the point contact geometry. This large-area filament is then formed by two independent interfaces, which confine the phase of stable high electron density. The position of these interfaces (filament boundaries) is approximately given by lines of constant local field strength of some specific value. A perpendicular cross section of the filamentary structure can be in a stationary state satisfactorily described by a simple one-dimensional model.

ACKNOWLEDGMENTS

The authors are indebted to S. Würfl, B. Finger, and A. Bernlochner for technical assistance and for providing some experimental data. We thank also E. Schöll, R. E. Kunz, and H. Kostial for helpful and stimulating discussions. Financial support by the Deutsche Forschungsgemeinschaft and the Deutscher Akademischer Austauschdienst is gratefully acknowledged.

* On leave from the Institute of Electrical Engineering of the Czech Academy of Sciences, Dolejškova 5, 182 02 Praha, Czech Republic.

[1] V.V. Vladimirov, A.F. Volkov, and E.Z. Mejlichov, *Plazma Poluprovodnikov* (Atomizdat, Moscow, 1979).
[2] E. Schöll and P.T. Landsberg, in *Proceedings of the 14th International Conference on Physics of Semiconductors, Edinburg, 1978*, edited by B.L.H. Wilson (Institute of Physics and Physical Society, Bristol, 1979).
[3] E. Schöll, Z. Phys. B **46**, 23 (1982).
[4] E. Schöll, Z. Phys. B **48**, 153 (1982).
[5] E. Schöll, *Nonequilibrium Phase Transitions in Semiconductors* (Springer, Berlin, 1987).
[6] D. Jäger, H. Baumann, and R. Symanczyk, Phys. Lett. A **117**, 141 (1986).
[7] F.-J. Niedernostheide, M. Arps, R. Dohmen, H. Willebrand, and H.-G. Purwins, Phys. Status Solidi B **172**, 249 (1992).
[8] K.M. Mayer, R. Gross, J. Parisi, J. Peinke, and R.P. Huebener, Solid State Commun. **63**, 55 (1987).
[9] K.M. Mayer, J. Parisi, and R.P. Huebener, Z. Phys. B **71**, 171 (1988).
[10] K. Aoki, U. Rau, J. Peinke, J. Parisi, and R.P. Huebener, J. Phys. Soc. Jpn. **59**, 420 (1990).
[11] A. Brandl, M. Völcker, and W. Prettl, Appl. Phys. Lett. **55**, 238 (1989).
[12] A. Brandl and W. Prettl, Festkörperprobleme **30**, 371 (1990).
[13] V. Novák and W. Prettl, in *Nonlinear Dynamics and Pattern Formation in Semiconductors and Devices*, edited by F.-J. Niedernostheide (Springer, Berlin, 1995).
[14] J. Spangler, B. Finger, C. Wimmer, W. Eberle, and W. Prettl, Semicond. Sci. Technol. **9**, 373 (1994).
[15] J.K. Pozhela, *Plasma and Current Instabilities in Semiconductors* (Pergamon, Oxford, 1981).
[16] G.A. Baraff, Phys. Rev. **128**, 2508 (1962).
[17] G. Hüpper, K. Pyragas, and E. Schöll, Phys. Rev. B **47**, 15 515 (1993).
[18] K. Küpfmüller, *Einführung in die theoretische Elektrotechnik*, 10th ed. (Springer, Berlin, 1973).
[19] A. Brandl and W. Prettl, Phys. Rev. Lett. **66**, 3044 (1991).
[20] W. Clauss, U. Rau, J. Peinke, J. Parisi, A. Kittel, M. Bayerbach, and R.P. Huebener, J. Appl. Phys. **70**, 232 (1991).
[21] G. Hüpper, K. Pyragas, and E. Schöll, Phys. Rev. B **48**, 17 633 (1993).
[22] T. Christen, Z. Naturforsch. Teil A **49**, 847 (1994).